Journal of Korean Powder Metallurgy Institute
Vol. 8, No. 3, 2001

Fabrication of Metallic Particle Dispersed Ceramic Based Nanocomposite Powders by the Spray Pyrolysis Process Using Ultrasonic Atomizer and Reduction Process

Y-H. Choa, B-H. Kim, Y-K. Jeong*, K-W. Chae, T. Nakayama***, T. Kusunose***, T. Sekino*** and K. Niihara*****

Division of New Materials Eng., Chonbuk National University, Chonbuk 561-756, Korea
**Korea Institute of Ceramic Engineering and Technology, Seoul 153-018, Korea*
***Dept. of Materials Sci. & Eng., Hoseo University, Chungnam 330-180, Korea*
****Institute of Scientific and Industrial Research, Osaka University, Osaka 567-0047, Japan*
(Received July 30, 2001)

Abstract MgO based nanocomposite powder including ferromagnetic iron particle dispersions, which can be available for the magnetic and catalytic applications, was fabricated by the spray pyrolysis process using ultrasonic atomizer and reduction processes. Liquid source was prepared from iron (Fe)-nitrate, as a source of Fe nano-dispersion, and magnesium (Mg)-nitrate, as a source of MgO materials, with pure water solvent. After the chamber were heated to given temperatures (500~800°C), the mist of liquid droplets generated by ultrasonic atomizer carried into the chamber by a carrier gas of air, and the mist was decomposed into Fe-oxide and MgO nano-powder. The obtained powders were reduced by hydrogen atmosphere at 600~800°C. The reduction behavior was investigated by thermal gravity and hygrometry. After reduction, the aggregated sub-micron Fe/MgO powders were obtained, and each aggregated powder composed of nano-sized Fe/MgO materials. By the difference of the chamber temperature, the particle size of Fe and MgO was changed in a few 10 nm levels. Also, the nano-porous Fe/MgO sub-micron powders were obtained. Through this preparation process and the evaluation of phase and microstructure, it was concluded that the Fe/MgO nanocomposite powders with high surface area and the higher coercive force were successfully fabricated.

Keywords : Nanocomposite powder, Fe/MgO system, Spray pyrolysis process, Magnetic property, High surface area

1. Introduction

Nanocomposite materials have recently been studied extensively[1-6] because of their potentials use in technology, such as high-density magnetic recording media, ferrofluids, catalysts, and so on. Various techniques such as vapor deposition,[7] r.f. sputtering,[8] reducing from metal oxide,[9] hydrothermal precipitation,[10] sol-gel method,[11,12] etc., have been employed to prepare ultrafine particles.

Among the variety of means to prepare nanocomposite materials, the spray pyrolysis process is one of the candidate processes, because the spray pyrolysis process using mist of liquid source is economical and effective to synthesize spherical and homogeneous powder in multi-component system compared to any other processes.[13,14] However, there has been not reported to prepare the nanocomposite particles by this way.

The Fe/MgO system under both reduced and oxidized forms has several applications in catalysis such as the synthesis of ammonia, organic synthesis and catalytic combustion. Furthermore, Fe/MgO composite system also has a potential for magnetic application, because pure Fe and oxidized Fe materials shows the good magnetic properties. For these applications, a high surface area support can influence the catalytic activity and the coercive force of iron by both physical effects, such as control of particle size or crystal morphology, and specific chemical effects, such as control of the oxidation state.

Therefore, in order to obtain suitable microstructure

for above interests, in this study, the Fe/MgO nanocomposite powders prepared by the spray pyrolysis process using ultrasonic atomizer and reduction processes. The purposes of the present work are to investigate the relationship between the powder preparation process and the microstructure of Fe/MgO nanocomposite powder and to evaluate the magnetic properties that closely relate to microstructure by several measurement techniques. The crystallographic structures and particle size of the samples were determined by X-ray diffractometry (XRD) and thermal gravity and hygrometry. Transmission electron microscopy (TEM) and scanning electron microscopy (SEM) observations were performed to observe the microstructure. The surface area and particle size were measured by BET method. The magnetic properties were measured using a SQUID magnetometer. To our knowledge, this is the first time that the metallic particle dispersed ceramic-based nanocomposite prepared by the spray pyrolysis process using ultrasonic atomizer and reduction processes has been reported.

2. Experimental Procedure

Fe-oxide/MgO powders were prepared using the modified ultrasonic spray process apparatus shown in Fig. 1. This apparatus composed of three zones. The first zone is the mist generating system of liquid source with ultrasonic atomizer. The second zone is the system of mist carriage with air carrier gas, mist vaporization and particle trap. The final zone is the pumping system of various gases produced in the process of the formation of powder and maintaining 1 atm.

Liquid source was prepared from dissolution of starting materials, $Mg(NO_3)_26H_2O$ and $Fe(NO_3)_39H_2O$ (Wako Pure Chemical Industries, Ltd., Japan), which weighted nitrate corresponding to 0, 5 and 20 vol% of metallic Fe particle in the final specimens (which denoted to SMF0, SMF5 and SMF20, respectively), in pure water to be 0.2 mol/l in concentration.

After the chamber and substrate were heated to given temperatures (500~800°C), the mist of liquid source was generated by ultrasonic atomizer with transducer operating at a frequency of 1.67 MHz, carried into the chamber by a carrier gas of air, vaporized in the chamber and trapped by filter under the atmosphere of air. All the procedure was done under the 1 atm. During this process, the mist was decomposed into Fe-oxide and MgO nano-powder (which denoted to OMF0, OMF5 and OMF20, respectively). The heat-treated sample in air atmosphere (chamber temperature) is marked with ending -A6, -A7 and -A8 (600, 700, and 800°C).

The obtained powders were reduced by hydrogen atmosphere (flow rate 0.5 l/min.) at 600~800°C. The reduced powders from OMF5 and OMF20 denoted to MF5 and MF20, respectively. The heat-treated sample in H_2 atmosphere is marked with ending -R6, -R7, and -R8 (600, 700 and 800°C).

The reduction behavior of Fe oxide was analyzed by

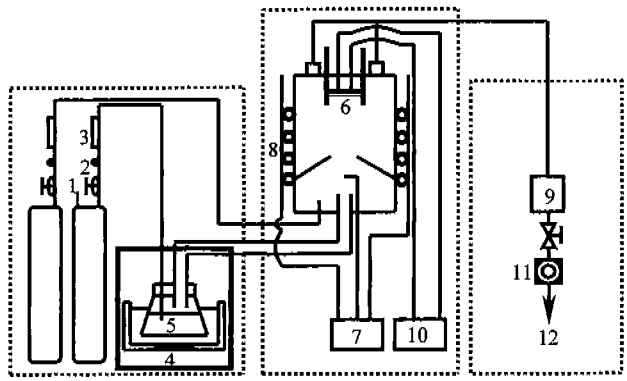

1.Regulator 2.Solenoid valve 3.Gas flow meter 4.Ultrasonic generator
5.Liquid source 6. Trapper/Filter 7.Temperature controller 8.Resistance heater
9.Particle trap 10. 9.11.12 11.Rotary vacuum pump 12.Exhaust gas

Fig. 1. Experimental set-up for ultrasonic spray pyrolysis process apparatus.

using the *in situ* measuring method[15], in which the hygrometry system for measuring the relative humidity of outlet gas was equipped with a TG system to monitor the progress of reduction reaction. The reduction experiment was conducted by raising the temperature to 1000°C with a heating rate of 10°C/min in a H_2 gas atmosphere (dew point -76°C, flow rate 0.5 *l*/min). The powder morphologies were observed by SEM (JSM-6400, JEOL, Japan) and TEM (H-8100, 200kV, Hithachi Ttd., Japan). The crystallographic structures and particle size of the samples were determined by XRD (Rigaku D/Max-3A) using Cu$K\alpha$ radiation. The surface area and particle size was measured by BET method using N_2 gas absorption. The magnetic properties were measured using a SQUID magnetometer with an applied magnetic field up to ±15000 gauss.

3. Results and Discussion

3.1. Fe-oxide/MgO nanocomposite prepared by the spray pyrolysis process

As presented schematically in Fig. 1, the powder particles were produced by passing ultrasonically atomized droplets of the above solutions through a heated tube flow reactor where pure water solvent evaporated, and subsequently the concentrated solution species reacted and solid particles were formed. An ultrasonic generator was utilized with an atomizing frequency of 1.67 MHz.

The average droplet diameter (mass mean diameter) can be estimated according to Lang[16]:

$$D_d = 0.34\ (8\pi\gamma / \rho f^2)^{1/3} \quad (1)$$

where, D_d is the droplet diameter, γ is the solution surface tension, ρ is the solution density, and f is the ultrasonic frequency applied.

For determination of the mean diameter of the particle (D_p) formed from the misted droplets, the following equation can be used[17];

$$D_p = D_d\ (C_{SMF}\ M_{OMF} / \rho_{OMF}\ M_{SMF})^{1/3} \quad (2)$$

The diameter of the misted droplets was calculated using the following parameters; $\gamma = 72.9 \times 10^{-3}$ N/m *(surface tension of pure water)*, $\rho = 1.011$ g/cm^3 for SMF5 and $\rho = 1.013$ g/cm^3 for SMF20, and f = 1.67 MHz. The obtained values of the mean diameter of the droplet are 2.945 μm and 2.94 μm, based on equation (1). Substituting these values in equation (2) and the corresponding constant for the pyrolysed system (precursor concentration $C_{SMF} = 0.2$ M, molecular mass (M_{OMF}) of the OMF5 and OMF20 are 49.26 and 74.19, the density (ρ_{OMF}) of the OMF5 and OMF20 are 3.842 and 4.366 g/cm^3, and molecular mass (M_{SMF}) of the precursor of the SMF5 and SMF20 are 267.80 and 298.31), theoretically expected values of particle diameter was 403.6 nm and 442.4 nm for OMF5 and OMF20, respectively.

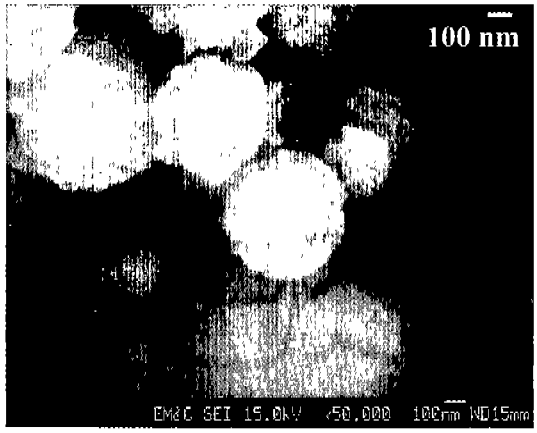

Fig. 2. The typical SEM micrograph for OMF20-A6 sample.

Figure 2 shows the typical SEM micrograph for OMF20-A6 sample. Experimentally determining value of the mean diameter for this sample was ~600 nm, and each aggregated powders composed of nano-sized Fe_2O_3/MgO materials. Comparison of the theoretically obtained results with the experimentally determined value, regardless of the equations being used for determination of the misted droplets (equation 1), undoubtedly shows that there is a substantially difference between the theory and the experiment. This is due to using the theoretical density of primary OMF particles packing. This fact shows that each secondary particle was not fully dense but porous.

For OMF20 sample series (OMF-A6 to OMF-A8), it was observed that the mean diameter for secondary aggregated particles was decreased with the increase of chamber temperature (the heat-treated sample in air atmosphere). This means that secondary aggregated particles composed of primary nano-Fe_2O_3-MgO particles was densified with increasing temperature by diffusion process.

XRD patterns for OMF20 samples with the chamber temperature are shown in Fig. 3. No reaction phases such as Mg-Fe spinel was observed in this experiment, and it was confirmed that OMF samples composed of

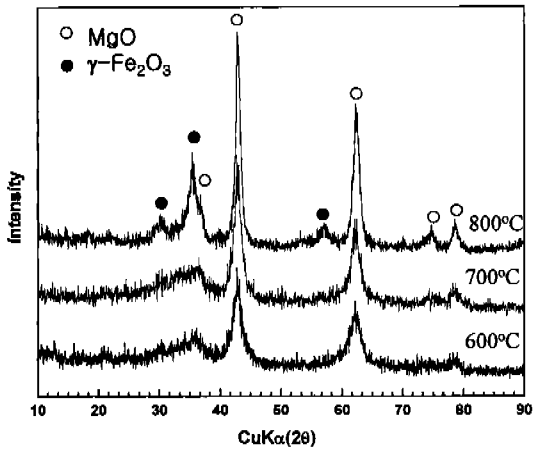

Fig. 3. XRD patterns for OMF20 samples with the chamber temperature.

γ-Fe_2O_3 and MgO. For OMF0 and OMF5 sample series, the similar trends of microstructure and particle size with chamber temperature were obtained.

3.2. Reduction of Fe-oxide/MgO nanocomposite and some properties

The reduction behavior was analyzed by using the hygrometry system for measuring the relative humidity of outlet gas, equipped with a TG system to monitor the progress of reduction reaction up to 1000°C with a heating rate of 10°C/min in a H_2 gas atmosphere. Fig. 4 shows the result of TG analysis of OMF20 powder during the heat up to 1000°C in H_2 atmosphere. The fractional weight loss gradually increases with increasing temperature and then rises abruptly at 250°C. Differential weight loss in Fig. 4 representing the

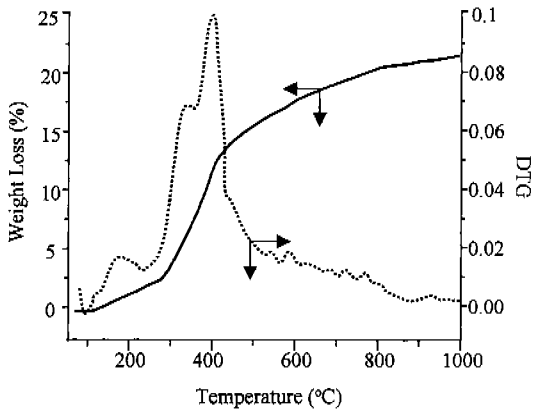

Fig. 4. TG and its differential curves of OMF20 sample during the heat up to 1000°C in H_2 atmosphere.

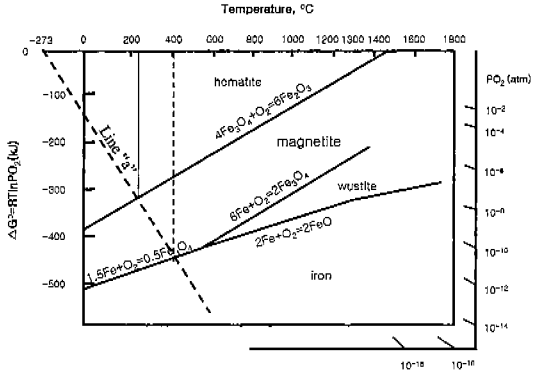

Fig. 5. The phase stability in the system Fe-Fe_2O_3 as a function of ΔG° and temperature.

reduction rate provides more details about the reduction process. Interestingly, it has been observed that the differential TG (DTG) curve comprises two peaks; one small peak below 200°C and the other large one in the temperature range of 250~500°C. The small peak might be due to the removal of adsorbed water molecules on the powder surface, while the large peak consisting of two overlapped peaks occurred because of the rapid reduction process of Fe_2O_3 in the OMF powder mixture.

Now the question arises why such an overlapped DTG peak occurred and whether this reduction behavior can be related to the formation kinetics of Fe nanoparticle from Fe_2O_3. This fact could be easily understood from thermodynamic consideration as shown in Fig. 5, which is the phase stability in the system Fe-Fe_2O_3 as a function of ΔG° and temperature. When the final phase of Fe was obtained at around 400°C, the reduction of Fe_2O_3 phase occurred by following the line "a". Therefore, the phase transformation of $Fe_2O_3 \rightarrow Fe_3O_4$ and $Fe_3O_4 \rightarrow Fe$ represented at ~250°C and ~400°C, respectively. The result of humidity analysis in Fig. 6 proves that the reduction reactions occurring in γ-Fe_2O_3 and MgO follow the reaction of $3Fe_2O_3 + H_2 \rightarrow 2Fe_3O_4 + H_2O$, and $Fe_3O_4 + 4H_2 \rightarrow 3Fe + 4H_2O$. Consequently, the occurrence of the overlapped peaks in OMF powder mixture is due to the formation of Fe nanoparticle from Fe_2O_3. Therefore, as considering the reduction behavior, the above obtained OMF5 and OMF20 powders were reduced by hydrogen atmosphere (flow rate 0.5 *l*/min) at 500~800°C for 1 h.

Figure 7 shows the TEM micrographs for the sample (MF20-A6-R6) after reducing OMF20-A6 at 600°C, in which the secondary aggregated particles was com-

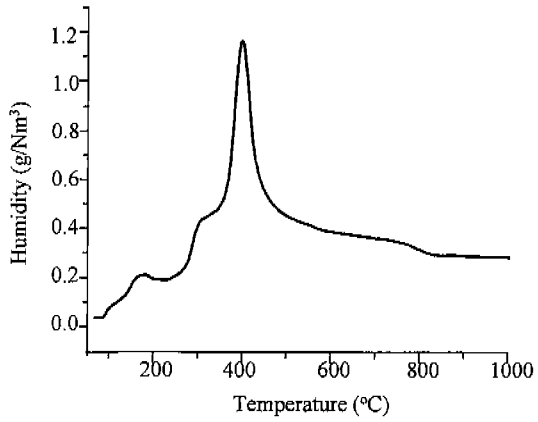

Fig. 6. Hygrometry curve for OMF20-A6 sample during the heat up to 1000°C in H_2 atmosphere.

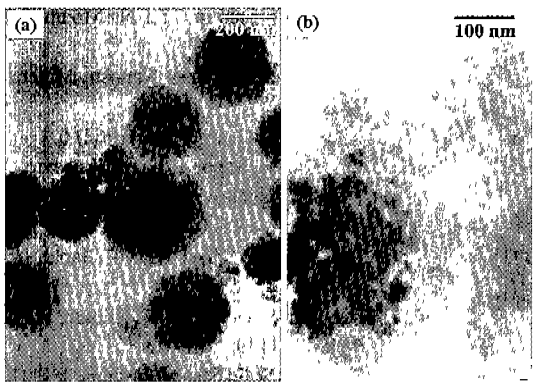

Fig. 7. TEM micrographs for the sample (MF20-A6-R6) after reducing OMF20-A6 at 600°C; (a) low magnification and (b) high magnification.

posed of primary nano-sized Fe, MgO and pore. For this sample, the particle size, specific surface area, and pore radius were determined by XRD using Scherrers formula and BET method using N_2 gas absorption. The particle size by XRD was 15.9 nm for Fe and 17.8 nm for MgO, and well coincide with the TEM observation as shown in Fig. 7. By BET method, the specific surface area was 23.5 m^2/g and the particle size calculated from the surface area and density was 57.4 nm. This difference between XRD result and BET result was caused by the principle of the measurement method. When the par-ticles formed aggregated, and contacted mutually, the surface area was decreased, and as a result, the particle size calculated from BET method was decreased. This means that this sample was aggregated as shown in Fig. 7 and porous as understood in the fact that the secondary particle size from TEM observation was ~300 nm. The average pore diameter measured by BET method was ~9 nm.

In the morphology for MF20-A5-R6, MF20-A7-R6 and MF20-A8-R6 samples with the different chamber temperature, the similar trends of relationship among microstructure, particle size and surface area were obtained. However, as increasing the chamber temperature, the particle size of Fe was increased. This means that secondary aggregated particles composed of primary nano-particles was densified and each particle was grown with increasing temperature. This fact was also observed for the samples with the different reduction temperature.

For the MF20-A6-R6 sample, a hysteresis loop of the *I-H* curve was obtained by SQUID magnetometer at 300 K, and the coercive force (*Hc*) is 680 gauss, which is approximately three orders of magnitude larger than that of pure iron metal (less than 1.0 gauss[18]). *Hc* is well known to be strongly dependent on the particle size and dislocation density.[19,20] When the particle size of a magnetic material decreased, its magnetic structure varies from a multi domain state to a single domain state, to reduce the total energy of the system; hence high *Hc* is presented.[20] The extremely high value of *Hc* was reported for particle size in the range of several 10 nm, with corresponds to the magnetic single domain structure. In this material, the size of iron particle lies in the a few 10 nm ranges and this Fe particle dispersoid might have a single domain structure. As increasing the chamber temperature and reduction temperature, the *Hc* was decreased (for example, the *Hc* of MF20-A6-R8 sample was 600 Oe). This result closely related to the change of Fe particle size with chamber and reduction temperature, as above mentioned.

4. Conclusions

MgO based nanocomposite powder with ferromagnetic nano-sized iron particle dispersions and high surface area, which can be available for the magnetic and catalytic applications, was prepared by the spray pyrolysis process using ultrasonic atomizer and reduction processes.

- Theoretical mean diameter for secondary aggregated particles was calculated. As compared with experimental results, the mean diameter for secondary aggregated particles was decreased with increasing the chamber temperature, because the secondary aggregated particles composed of primary nano-Fe_2O_3-MgO particles were

densified with increasing temperature by diffusion process.

- The reduction behavior was analyzed by using the hygrometry with a TG system. As compared with thermodynamic data, it is confirmed that the reduction of Fe-oxide/MgO to Fe/MgO was occurred with the phase transformation of $Fe_2O_3 \rightarrow Fe_3O_4 \rightarrow Fe$.

- From the TEM, BET and XRD results, it was confirmed that the secondary aggregated particles were composed of primary nano-sized Fe, MgO and pore. The primary particle size of each phase was a few 10 nm range. With increasing the reduction temperature, the mean particle size was increased.

- The extremely high coercive force was obtained at room temperature, which is approximately three orders of magnitude larger than that of pure iron metal and strongly dependent on the change of ferromagnetic iron particles.

Acknowledgment. This work is supported by research funds of Chonbuk National University.

References

1. T. Nakayama, Y. H. Choa, T. Sekino and K. Niihara: J. Ceram. Soc. Jap., **108** (2000) 781.
2. A. Chatterjee and D. Chakravorty: Appl. Phys. Lett., **60** (1992) 138.
3. S. Roy, D. Das, D. Chakravorty and D. C. Agrawal: J. Appl. Phys., **74** (1993) 4746.
4. T. K. Kundu and D. Chakravorty: J. Mater. Res., **9** (1994) 2480.
5. J. P. Wang, D. H. Han, H. L. Luo, N. F. Gao and Y. Y. Liu: J. Magn. Magn. Mater., **135**(1994) L251.
6. T. K. Kundu and D. Chakravorty: Appl. Phys. Lett., **66** (1995) 3576.
7. C. G. Granqvist and O. Hunderi: Phys. Rev. B., **16** (1977) 3513.
8. B. Abeles, P. Sheng, M. D. Coutts and Y. Arie: Adv. Phys., **24** (1975) 407.
9. M. Guglielmi and G. Principi: J. Non-cryst. Solids, **48** (1982) 161.
10. Y. Shang and G. V. Weert: Hydrometallurgy, **33**(1993) 273.
11. R. A. Roy and R. Roy: Matter. Res. Bull., **19** (1984) 169.
12. J. P. Wang and H. L. Luo: J. Magn. Magn. Mater., **131** (1994) 54.
13. J-H. Lee, B.-H. Kim, E.-S. Choi, and J.-S. Hwang: J. Kor. Ceram. Soc., **30** (1993) 325.
14. B-H. Kim, K. Ueda, O. Sakurai and N. Mizutani: J. Ceram. Soc. Jap., **100** (1992) 246.
15. T. H. Kim, J. H. Yu, and J. S. Lee: Nanostr. Mater., **9** (1997) 213.
16. R.J. Lang: J. Acoustical Soc. Amer., **34** (1962) 6.
17. J. M. Nedeljkovie, Z. V. Saponjic, Z. Rakocevic, V. Jokanovic and D. P. Uskokovic: Nanostr. Mater., **9** (1997) 125.
18. H. Kaneko and M. Honma: "Zisei Zairyo", Japan Inst. Metals., (1997) 143.
19. T. Sekino, T. Nakajima, S. Ueda and K. Niihara: J. Am. Ceram. Soc., **80** (1997) 1139.
20. R. Kamel and A. Reffat: Solid State Commun., **8** (1970) 821.